· Arcticle ·
doi: 10.13679/j.advps.2014.4.00222

Advances in Polar Science
December 2014 Vol. 25 No. 4: 222-233

Links between Arctic sea ice and extreme summer precipitation in China: an alternative view

Petteri Uotila*, Alexey Karpechko & Timo Vihma

Finnish Meteorological Institute, FI-00101 Helsinki, Finland

Received 9 June 2014; accepted 14 November 2014

Abstract Potential links between the Arctic sea-ice concentration anomalies and extreme precipitation in China are explored. Associations behind these links can be explained by physical interpretations aided by visualisations of temporarily lagged composites of variables such as atmospheric mean sea level pressure and sea surface temperature. This relatively simple approach is verified by collectively examining already known links between the Arctic sea ice and rainfall in China. For example, similarities in the extreme summer rainfall response to Arctic sea-ice concentration anomalies either in winter (DJF) or in spring (MAM) are highlighted. Furthermore, new links between the Arctic sea ice and the extreme weather in India and Eurasia are proposed. The methodology developed in this study can be further applied to identify other remote impacts of the Arctic sea ice variability.

Keywords **Self-Organising Maps, atmospheric large-scale circulation, precipitation, sea surface temperature, surface air temperature, sea ice, Arctic, China**

Citation: Uotila P, Karpechko A, Vihma T. Links between Arctic sea ice and extreme summer precipitation in China: an alternative view. Adv Polar Sci, 2014, 25: 222-233, doi:10.13679/j.advps.2014.4.00222

1 Introduction

The extent and thickness of Arctic sea ice have dramatically decreased over the past few decades, particularly in summer and early autumn. This decline is related to anthropogenic warming and increased poleward oceanic and atmospheric heat transport from mid-latitudes, and it has been further accelerated by feedback processes related, among others, to surface albedo, water vapour and clouds, and increased heat flux from the open ocean to atmosphere[1-4].

Due to the positive feedback processes the Arctic has warmed at a higher rate than mid-latitudes, which in turn has decreased the meridional temperature gradient in between the two[5]. Hence, it has been hypothesised that the Arctic warming along with decreased sea ice is possibly impacting the mid-latitude climate by changing the strength, position and persistence of major storm tracks. These features affect climate extremes which cause local havoc and therefore it is important to understand how the Arctic sea-ice cover is associated with climate extremes, often quantified as indices based on temperature and precipitation events. Close relationships between storms and large-scale circulation are evident[6], but due to the high natural variability of the large-scale atmospheric circulation, its relationship between the declining Arctic ice has not been definitively linked[7]. Therefore new useful approaches are urgently needed to determine possible linkages between Arctic sea ice and large-scale atmospheric circulation. One of these approaches, which we utilize in this paper, is based on simple visualisation of relationships between variables.

In this study, we address linkages between rapidly changing Arctic sea ice and climate extremes in East Asia, particularly in China. Four studies, reviewed next, have already explored these linkages in terms of rainfall and we will use their results to support our approach which in turn provides a somewhat alternative and to some extent clearer view on how Arctic sea-ice anomalies are related to climate extremes in China (Table 1).

* Corresponding author (email: petteri.uotila@fmi.fi)

Table 1 Effects of Arctic sea-ice anomalies on the summer rainfall in China as suggested by previous studies and this study. Sea-ice regions are abbreviated as: BOS=Bering-Okhotsk Sea, GS=Greenland Sea, LS=Labrador Sea and PA=Pan-Arctic

Study	Region	Years	Season	Results	Notes
Zhao et al. (2004)[8]	BOS	1971-1999	MAM	Reduced sea-ice extent leads to an enhanced summer (JJ) monsoon rainfall in southeastern China.	Rainfall from meteorological stations, and atmospheric temperature and wind fields from NCEP1. Some sea-ice–rainfall linkages appear more dominant than in subsequent studies probably due to methodical differences.
Wu et al. (2009)[9]	GS	1968-2005	MAM	Decreased (increased) SIC corresponds to increased (decreased) summer (JJA) rainfall in Northeast and central China and decreased (increased) summer rainfall in South China.	Rainfall from meteorological stations, and atmospheric pressure and wind fields from NCEP1. Results seem consistent with subsequent studies.
Guo et al. (2013)[10]	PA	1979-2009	MAM	Reduced sea ice leads to an enhancement of summer (JJA) rainfall in Northeast China. Concurrently, the rainfall over Meiyu-Changma-Baiu front significantly decreases.	Rainfall from CMAP observational analysis, and atmospheric pressure and wind fields from NCEP1. Results seem consistent with subsequent studies.
Wu et al. (2013)[11]	LS	1979-2013	DJF	Corresponding to a heavy SIC, increased summer (JJA) rainfall is observed from north of Europe extending southeastwards to the mid-latitude East Asia.	Rainfall from global observational analysis of Chen et al.[12], and atmospheric pressure and wind fields from NCEP1 and JRA-25 reanalyses. Results seem consistent with subsequent studies.
This study	PA	1979-2013	MAM, DJF	Decreased (increased) SIC in BOS (LS) in MAM and DJF leads to increased rainfall in Northeast China and decreased rainfall in Southeast China in summer (JJA). The opposite rainfall response occurs when SIC decreases (increases) in BOS (LS).	Rainfall data from HadEX2 extreme indices data set. ERA-Interim pressure and temperature fields. Results seem consistent with subsequent studies.

First, Zhao et al.[8] found that sea-ice extent anomalies in the Sea of Okhotsk and in the Bering Sea in spring (MAM) are associated with extreme summer (JJ) monsoon rainfall in southeastern China. Their results were based on observational analysis, NCEP1 reanalysis, and model simulations. According to their study, a reduced spring sea-ice extent resulted in an enhanced monsoon due to changed atmospheric circulation caused by stationary wave dynamics and soil moisture anomalies. In spring, the reduced sea-ice extent in the Sea of Okhotsk and the Bering Sea triggers an eastward propagating wave and anomalous high over Europe which in turn reduces the precipitation and soil moisture in Europe. In summer, the dryer European soil warms up more effectively and promotes stationary atmospheric waves which cause a persistent high pressure anomaly in East Asia. This high pressure anomaly increases cold air flow from the north which keeps the Asian summer monsoon and the associated frontal structure more south hence increasing rainfall in southeastern China. We show that our approach can reveal a relationship between the spring sea-ice concentration anomalies (SICA) and summer rainfall extremes. Additionally, we will illustrate differences in the evolution of atmospheric circulation anomaly composites from spring to summer related to spring SICA.

Second, Wu et al.[9] found a statistically significant link between the sea-ice concentration in the Arctic Ocean, particularly in the Greenland Sea, in spring (MAM) and rainfall in China in the following summer (JJA) based on NCEP1 reanalysis and rainfall observations from 1968−2005. They showed that negative SICAs were linked to increased summer rainfall in Northeast and central China and to decreased summer rainfall in South China, while the opposite was true for positive SICAs. Wu et al.[9] attributed rainfall anomalies in China to two wave trains: one meridional dipole structure over East Asia and another one originating in northern Europe extending to the Korean Peninsula. These wave train structures might be triggered by persisting spring-to-summer SICAs and Eurasian snow cover anomalies. Surface anomalies such as these impact the subpolar westerlies and the redistribution of Rossby waves.

Third, Guo et al.[10] analysed linkages between the spring Arctic sea ice and the East Asian Summer monsoon using Empirical Orthogonal Functions and numerical model experiments. Their analysis revealed a mediating role of the North Pacific sea surface temperature (SST) changes which were consistent with changes in large-scale atmospheric circulation and precipitation. They found that reduced spring Arctic sea ice leads to an enhanced summer rainfall in Northeast China, while, concurrently, the rainfall over Meiyu-Changma-Baiu front in southern China decreases.

To summarise, their results confirmed that the spring Arctic sea-ice anomalies affect the atmospheric circulation which modifies SSTs in North Pacific. These temperature anomalies persist until summer and influence the summer monsoon circulation and rainfall in East Asia. To simulate this mechanism, a coupled atmosphere-ocean model is needed because of the interaction between the atmospheric circulation and SST in the North Pacific. We show that our approach reveals the linkage between the spring Arctic sea ice and summer rainfall in China as found by Guo et al.[10].

Fourth, Wu et al.[11] published a study where they analysed NCEP1 and JRA-25 reanalyses from 1979−2010. They found that winter SICAs in the Labrador Sea along the eastern coast of Newfoundland correlated with summer atmospheric circulation anomalies over north Eurasia, including China. Furthermore, related summer rainfall variability over a region extending southeastward from northern Eurasia to the mid-latitude East Asia was influenced so that heavy sea-ice winters were followed by increased summer rainfall over the region. These observational results were in line with the atmospheric ECHAM5 model sensitivity experiments. Accordingly, winter SICAs west of Greenland are a possible precursor for summer rainfall anomalies over China. Also, this relationship will be tested with our approach.

Four studies cited above demonstrate that complex interactions between several components of the climate system (ocean, sea ice, atmosphere and land) with intra-seasonal response times are required to produce the mid-latitude response to high-latitude anomalies. Mechanisms used to explain links between sea ice in different Arctic regions and rainfall in China vary between studies being either related to the Atlantic SSTs, the Pacific SSTs, European soil water content or persistence of Arctic sea-ice and Eurasian snow cover anomalies. The persistence of these factors triggers atmospheric Rossby wave train responses later in summer, which, by changing the atmospheric circulation, modify the rainfall in China. However, a comprehensive picture of the rainfall response in China remains either obscure or even contradictory, as seen from Table 1, probably due to differences in methodologies, and selected regions and time periods. For example, Zhao et al.[8] associate reduced Arctic sea ice with enhanced summer rainfall in southeastern China while Wu et al.[11] argue that summer rainfall in southern China decreases along with the Arctic sea ice in winter. Issues such as these require clarification.

Hence, finding robust mechanisms to explain as elegantly as possible the mid-latitudinal response is quite challenging. Furthermore, a simplification of visualisation, if possible, of already hypothesized mechanisms is desirable because it makes their comprehension and verification easier. This is the main aim of this study−to verify that our relatively simple visualisation approach can capture the essential features of four hypothesized links between the Arctic sea ice and the East Asian rainfall. If successful, we will expand our approach to explore other links between the Arctic sea ice and weather extreme indices related to precipitation and temperature in future studies.

2 Methods and Data

We use the method of Self-Organising Maps[13] (SOMs) to classify Arctic SICA patterns and to associate these patterns with a range of variables such as extreme weather indices. The SOM algorithm converts nonlinear statistical relationships between high-dimensional data into simple geometric relationships of their image points on a low-dimensional display, usually a regular two-dimensional grid of nodes. In our case, these nodes are geographical surface maps of geophysical variables. The SOM algorithm is based on an unsupervised learning process to produce this low-dimensional representation of the training data samples. Importantly, the SOM algorithm places more nodes in the areas of high-input-data density and thus attempts to preserve the probability density function of the input data. The SOM technique does not need a priori decisions on data structure but is trained when processing the data itself, unlike other similar clustering techniques. Due to these properties, the SOM technique is especially suitable for visualizing high-dimensional data.

Kohonen published a detailed description of the SOM algorithm[13], and a paper by Hewitson and Crane[14] provides more information on the application of SOMs to climate data. SOMs have been well tested in many climatic studies and have proven to be a very useful method to obtain and visualise a small number of patterns from large data sets (see for example[15-18]). In earlier studies, we have found that the SOM technique is suitable for the creation of synoptic climatologies of the polar regions[15-16]. In these studies SOMs consist of a two-dimensional grid of nodes, typically seven times five nodes, where each node represents a circulation pattern. In this analysis, our approach in general follows Alexander et al.[19], who applied SOM to classify global SST patterns. Here we apply SOMs to produce five Arctic sea-ice concentration anomaly (SICA) patterns (Figure 1).

In Figure 1, the SOM nodes are presented in a regular array, which do not correspond to the quantitative measure of similarity between the nodes. Initially, we generated SOM arrays of different sizes and after comparing these arrays we found SOMs consisting of five SICA patterns suitable for our analysis since they very compactly display relationships between regional SICA features. For example, arrays of three SICA patterns do not show intermediate SICA patterns, such as (3,0) in Figure 1 where a positive SICA in the Barents Sea occurs with a negative SICA in the Labrador Sea. As explained in the Results section, these intermediate patterns are important to explain rainfall anomalies in China in the following summer. On the other hand, we find that a larger number of nodes does not produce distinctly different SICA patterns compared to the five nodes in Figure 1. At the same time the number of months mapped to nodes becomes too small to be statistically representative. Hence we chose five node array SOMs for our analysis. Our main results

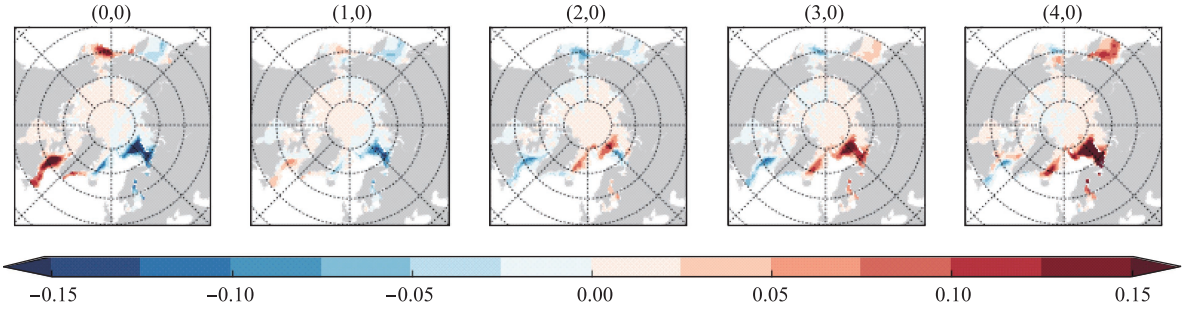

Figure 1 A five node Self-Organising Map of spring (MAM) Arctic sea-ice concentration anomaly (SICA) based on detrended HadISST data from 1979−2013. Units are dimensionless. The first SOM pattern on the left (0,0) represents opposite SICA conditions than the last SOM pattern on the right (4,0). SOM patterns between: (1,0), (2,0) and (3,0) represent intermediate SICA conditions. Ocean grid cells without sea ice are white while land areas are grey.

and conclusions, however, do not depend on, for example, whether one uses five or seven node SOMs, and are in this sense robust.

We generated a spring (MAM) and winter (DJF) SOMs using linearly detrended monthly Arctic SICAs based on HadISST data set from 1979−2013[20]. Sea ice concentration data are mapped onto a 1°×1° latitude/longitude grid. Since the HadISST inception, the SIC data have been widely and successfully used for both observation-based research and model simulations. Sea surface temperature (SST) data are taken from the UK Met Office Marine Data Bank (MDB), which from 1982 onwards also includes data received through the Global Telecommunications System. In order to enhance the HadISST data coverage, monthly median SSTs for 1871−1995 from the Comprehensive Ocean-Atmosphere Data Set (ICOADS) were also used where there were no MDB data. The sea-ice data are taken from a variety of sources including digitized sea-ice charts and passive microwave retrievals. HadISST temperatures are reconstructed using a two-stage reduced-space optimal interpolation procedure, followed by superposition of quality-improved gridded observations onto the reconstructions to restore local detail. The sea-ice fields are made more homogeneous by compensating satellite microwave-based sea-ice concentrations for the impact of surface melt effects on retrievals in the Arctic and for algorithm deficiencies in the Antarctic, and by making the historical *in situ* concentrations consistent with the satellite data. SSTs near sea ice are estimated using statistical relationships between SST and sea-ice concentration. Due to the careful processing of HadISST data, which uses all available data and takes into account issues with data coverage and homogenisation, we argue that the HadISST data are suitable in terms of their consistency for the SOM analysis during the analysis period which covers the satellite era.

The reason for removing trends from the data is so that changes observed from one state to another reflect the actual variability of the SICA patterns rather than long-term trends toward the warming Arctic Ocean. Analogously to Wu et al.[9,11], we define DJF as winter, MAM as spring and JJA as summer. As explained earlier, MAM and DJF SOMs consist of five SICA patterns. Because the SOM method associates each monthly SICA record to the closest SICA SOM pattern by finding the one with the minimum root-mean-square difference, we can temporally relate SICA patterns with any meteorological variable. Although the filtering of SOM MSLP pattern time series has proven to be desirable when associated with rainfall trends due to mismatches between some patterns and the original data[21], in our case the filtering is not essential. This is because we classify large-scale SICA patterns, where small scale variability is not important, unlike in MSLP patterns where cyclones are related to large rainfall events, and because we explore physical relationships between SICA patterns and extreme rainfall indices, not their trends.

We use the gridded land-based HadEX2 dataset of indices of temperature and precipitation extremes[22]. HadEX2 currently represents the most comprehensive global gridded dataset of temperature and precipitation extremes based on daily *in situ* data available. Indices were calculated based on station data, resulting in the production of 17 temperature and 12 precipitation indices derived from daily maximum and minimum temperature and precipitation observations. High-quality *in situ* observations from over 7 000 temperature and 11 000 precipitation meteorological stations across the globe were obtained to calculate the indices over the period of record available for each station. HadEX2 indices were interpolated onto a 3.75°×2.5° longitude/latitude grid over the period 1901−2010.

We chose an extreme precipitation index for this study index because we wanted to compare our results with precipitation based results from literature, as explained in Introduction. We plan to analyse other HadEX2 indices with the method presented in this paper, but to demonstrate the applicability of our method here we only used one precipitation index. The monthly maximum consecutive 5 day precipitation (RX5day) index and the monthly maximum consecutive 1 day precipitation (RX1day) index are the only precipitation indices available for sub-annual time scales. We decided to use the RX5day index, because a slightly larger number of stations were used to produce it than the RX1day index.

Specifically, we relate SICA patterns from 1979−2010 to HadEX2 RX5day index, with 2 metre surface air temperature (SAT) fields, sea surface temperature fields (from HadISST) and with atmospheric circulation composites based on the monthly mean sea level pressure (MSLP) fields. Meteorological MSLP and SAT data are based on ERA-Interim re-analysis product[23]. ERA-Interim is a global atmospheric reanalysis from 1979, continuously updated in real time. The data assimilation system used to produce ERA-Interim is based on a 2006 release of the Integrated Forecasting System (Cy31r2). The system includes a 4-dimensional variational analysis (4D-Var) with a 12-hour analysis window. The spatial resolution of the data set is approximately 80 km (T255 spectral) on 60 vertical levels from the surface up to 0.1 hPa. ERA-Interim provides realistic estimates for the atmospheric circulation and cyclones in the Northern Hemisphere[24] in the Arctic. In terms of Arctic warming, recent observational estimates and reanalysis products agree reasonably well with the ERA-Interim reanalysis for this region[25]. Cornes and Jones[26] also show that trends in mean values and in temperature extremes are successfully replicated in the ERA-Interim reanalysis in data-rich areas such as Europe. Accordingly, ERA-Interim is one of the best reanalysis products for use in our study.

We visualise MSLP anomaly (MSLPA), SICA, SAT anomaly (SATA) and SST anomaly (SSTA) composites by temporally preceding and lagging the month of SICA patterns, which provides us an opportunity to analyse any physically sensible relationships appearing. These visualised relationships between SICA patterns and MSLPA, SICA, SATA and SSTA composites are used to interpret and reason whether relationships between the Arctic SICAs and East Asian climate extremes are physically reasonable, robust and significant.

3 Results

3.1 The SOM based on sea ice concentration anomalies in MAM

A five-pattern SOM based on SICA in MAM is presented in Figure 1. Figure 1 illustrates strength of SOM analysis as the SICA patterns are automatically ordered from negative to positive following as closely as possible the distribution of input data. This visualisation feature helps the interpretation of data set. The first pattern on the left (0,0) represents strongly positive SICAs in the Bering Sea and in the Labrador Sea while negative SICAs are apparent in the Greenland Sea, in the Barents Sea and in the Sea of Okhotsk. The second pattern from the left (1,0) looks similar to (0,0) pattern, but now SICAs are smaller in terms of their absolute values except in the Sea of Okhotsk. Gradually changing SICA patterns from left to right are further highlighted in pattern (2,0) where SICAs in the Bering Sea and in the Labrador Sea have become weakly negative, and SICAs in the Greenland Sea and in the Barents Sea weakly positive. In pattern (3,0), SICAs in the Bering Sea and in the Labrador Sea are negative and in the Sea of Okhotsk, the Barents Sea and the Greenland Sea positive which is opposite than the SICA pattern (0,0). Finally, pattern (4,0) resembles pattern (3,0) except anomalies are stronger, particularly in the Sea of Okhotsk, although now the negative SICA in the Labrador Sea is weaker than in (3,0). Furthermore, the SICA in the Bering Sea has a positive/negative dipole pattern. To summarise, the strongest signals of SICA variability in MAM originate from the marginal Arctic Seas primarily from the Sea of Okhotsk, the Bering Sea, the Labrador Sea, the Barents Sea and the Greenland Sea.

3.2 Rainfall in JJA associated with the MAM sea ice concentration anomaly SOM

In Figure 2 extreme precipitation events over Asia in JJA are associated with MAM SICA patterns of Figure 1. The weakest SICA pattern (2,0), is associated with the weakest rainfall anomaly response, while the stronger SICA patterns are associated with stronger RX5day rainfall anomaly responses. This difference emphasises the linkage between the spring Arctic sea ice and summer rainfall in China. The strongest rainfall anomalies in China are related to SICA patterns (1,0), (3,0) and (4,0) which show mutual sea ice variability predominantly in the Bering Sea, the Sea of Okhotsk and the Labrador Sea. This variability highlights the importance of these regions for the summer rainfall in China. On the other hand, if the Arctic sea ice variability over the whole Arctic Ocean was the major driver of rainfall variability, one could expect the largest difference between (0,0) and (4,0) because these SICA patterns are mutually the most opposite. However, rainfall anomaly composites (3,0) and (4,0) show the largest mutual difference, which is related to the subtropical Pacific SSTAs as we will demonstrate section 3.4.

According to Zhao et al.[8] reduced sea-ice extent in the Bering Sea and Sea of Okhotsk leads to enhanced summer rainfall in Southeast China. This is somewhat apparent when we compare the precipitation composite (2,0) of Figure 2, which is associated with negative SICA patterns in the Bering Sea and in the Sea of Okhotsk (Figure 1), with the precipitation composite (3,0) of Figure 2, which is associated with a positive SICA pattern in the Sea of Okhotsk and with a weakly negative SICA in the Bering Sea (Figure 1). Consistent with Zhao et al.[8], the precipitation anomaly (3,0) is more negative than the precipitation anomaly (2,0) in Southeast China. Furthermore, the precipitation anomaly (3,0) is positive in Northeast China indicating a northward shift of the monsoon associated frontal structure.

Our results are consistent with Zhao et al.[8] in the sense that both studies show relationships between SICA and precipitation, but not all results of Zhao et al.[8] are straightforward to derive using our method. For example,

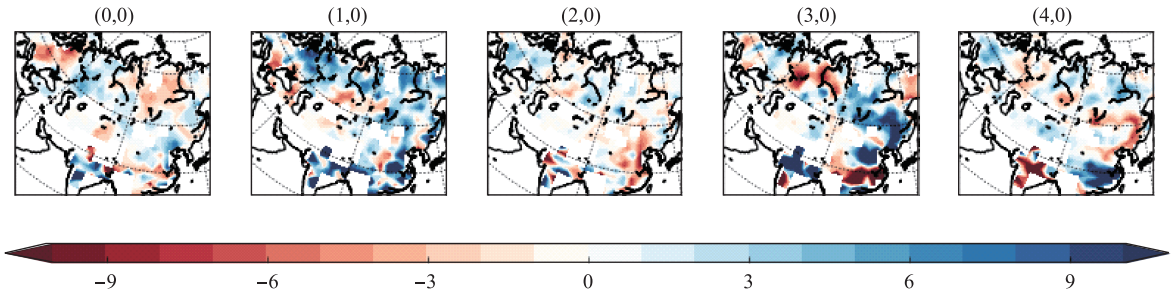

Figure 2 Detrended monthly maximum consecutive 5 day precipitation (HadEX2 RX5day index in mm) anomalies in JJA mapped to SOM patterns in Figure 1 using three months lag time. White areas indicate inadequate data for the computation of RX5day index. Details of the HadEX2 product can be found from Donat et al.[22].

Zhao et al.[8] conclude that reduced sea-ice extent in the Bering Sea and Sea of Okhotsk leads to enhanced summer rainfall in Southeast China. As explained in the previous paragraph this conclusion is consistent with our approach when comparing SICA patterns (2,0) and (3,0), and associated rainfall composites. On the contrary, our method indicates the opposite when, for example, comparing the extreme rainfall composites (2,0) and (4,0) associated with negative and positive SICAs in the Bering Sea and Sea of Okhotsk, respectively. Reasons for this disagreement seem mainly methodical: Zhao et al.[8] defined two sea-ice categories, heavy and light sea-ice years, while we define five SICA patterns; they analysed JJ rainfall composites from 1971-1999 using the Bering Sea and the Sea of Okhotsk sea-ice extent only, not JJA rainfall anomalies from 1979-2013 and not the whole Arctic sea-ice concentration as we do; and most importantly, Zhao et al.[8] specifically separated the impact of the Bering Sea and the Sea of Okhotsk sea ice on the rainfall in Southeast China, while our method takes simultaneously into account impacts of other sea-ice regions, such as the Barents and Greenland seas and the Labrador Sea. In summary, considering longer time series and taking into account the whole Arctic sea ice variability reveals some disagreements with Zhao et al.[8]. Although some of the linkages reported by them can also be found with our method, they do not seem dominant compared to linkages revealed by others as explained below.

Wu et al.[9] and Guo et al.[10] found that reduced Arctic sea ice, particularly in the Greenland Sea, leads to an increased summer rainfall in Northeast China while the opposite is true in South China. This linkage becomes clear when comparing rainfall composites associated with reduced, the pattern (0,0) of Figure 1, and increased, the pattern (4,0) of Figure 1, sea-ice conditions in the Barents and Greenland seas, respectively. Consistent with Wu et al.[9] and Guo et al.[10], pattern (0,0) shows an increased rainfall in Northeast China and a reduced rainfall in Southeast China, while (4,0) shows the opposite response. This contrast in rainfall responses between Northeast and Southeast China is very clear in composite (4,0). A similar rainfall response can also be seen when comparing rainfall composites associated with SICA patterns (3,0) and (4,0), where SICA patterns look rather similar, but their positive anomalies are smaller in (3,0) than in (4,0). This rather uniform Arctic-wide difference between (3,0) and (4,0) will be linked to the associated change in rainfall in terms of large-scale atmospheric circulation and persistence of SST anomalies in the following two sections 3.3 and 3.4. Overall, our results are generally consistent with[8-10].

Systematic differences of extreme rainfall events associated with SICA patterns in MAM emerge also elsewhere in Eurasia as seen in Figure 2. Notably, the Indian subcontinent shows a strong response reminiscent to the one in China (composites (3,0) and (4,0)). Additionally, opposite responses, resembling the opposite ones in Northeast China and Southeast China are visible in northeast and southeast Europe between composites (0,0) and (4,0). Dipole responses such as these indicate shifts of major atmospheric frontal structures or storm tracks, and deserve further studies.

3.3 Sea ice concentration, atmospheric circulation and surface temperatures in MAM

The strength of the northern hemisphere storm track can be characterised by the meridional pressure gradient between mid-latitudes and high latitudes. The most well-known index that measures this difference is the North Atlantic Oscillation Index which is the atmospheric pressure difference between Iceland and the Azores at the sea level[27]. Another, a more hemisphere-wide is the Arctic Oscillation which correlates well with the North Atlantic Oscillation[28]. Generally, when the height difference of atmospheric pressure levels between the high latitudes and the mid-latitudes is increased, the storm track strengthens and the large-scale flow becomes more zonal than the average.

High sea-ice conditions, i.e. positive SICAs, patterns (3,0) and (4,0) in Figure 1, in the Barents Sea and in the Sea of Okhotsk are characterised by positive MSLP anomalies (MSLPA) over the Arctic and negative MSLPAs over the north Atlantic and east Siberia (Figure 3, the second row from top, two rightmost panels). During these MSLPA composites, SICAs are negative in the Labrador Sea and in the Bering Sea. On the contrary, negative MSLPAs over the Arctic, and positive MSLPAs over the north Atlantic and east Siberia are

related to negative SICA patterns in the Barents Sea and the Sea of Okhotsk while positive SICA patterns occur in the Labrador Sea and in the Bering Sea (Figure 3, the second row from top, two leftmost panels).

When positive a MSLPA prevails over the north Atlantic and a negative one over the Arctic, the sea-ice formation increases and melting decreases in the Labrador Sea due to enhanced flow of near-surface cold winter air from the Arctic to the Labrador Sea (Figure 3, two topmost rows and two leftmost panels). The positive MSLPA over east Siberia has a similar positive impact for the sea conditions in the Bering Sea. On the contrary, a positive MSLPA over the Arctic and a negative MSLPA over east Siberia results in a cold air flow to the Sea of Okhotsk (Figure 3, two topmost rows and two rightmost panels). In the Barents and Greenland seas, the cold air flow is increased when a positive MSLPA over the Arctic and a negative MSLPA over the north Atlantic occur.

When the MSLPA in the north Atlantic is positive and the MSLPA in the Arctic is negative, sea ice in the Barents and Greenland seas is reduced. In the Barents Sea, negative SICAs occur when the east Siberian MSLPA is negative indicating a larger amount of cyclones entering the region with increased heat and precipitation. Related to these responses, negative sea-ice anomalies occur in the Sea of Okhotsk when the MSLPA is negative in the Arctic and positive over east Siberia (Figure 3, two topmost rows and two leftmost panels). As in the Barents Sea, these MSLPA anomalies enhance the flow of warm marine air to the region, in this case from the Pacific. In the Labrador Sea, the negative (positive) north Atlantic MSLPA enhances warm marine (cold polar) air flow to the region reducing (increasing) the amount of ice (Figure 3, two topmost rows). Generally, positive (negative) SICAs in Figure 1 are associated with negative (positive) SATAs (Figure 4). Because atmospheric conditions resembling the ones in MAM prevail already in FMA, i.e. before MAM SICA conditions, we can confirm that the atmospheric flow anomalies are the primary driver of the Arctic sea-ice variability in general and in this case in MAM (Figure 3, the top row).

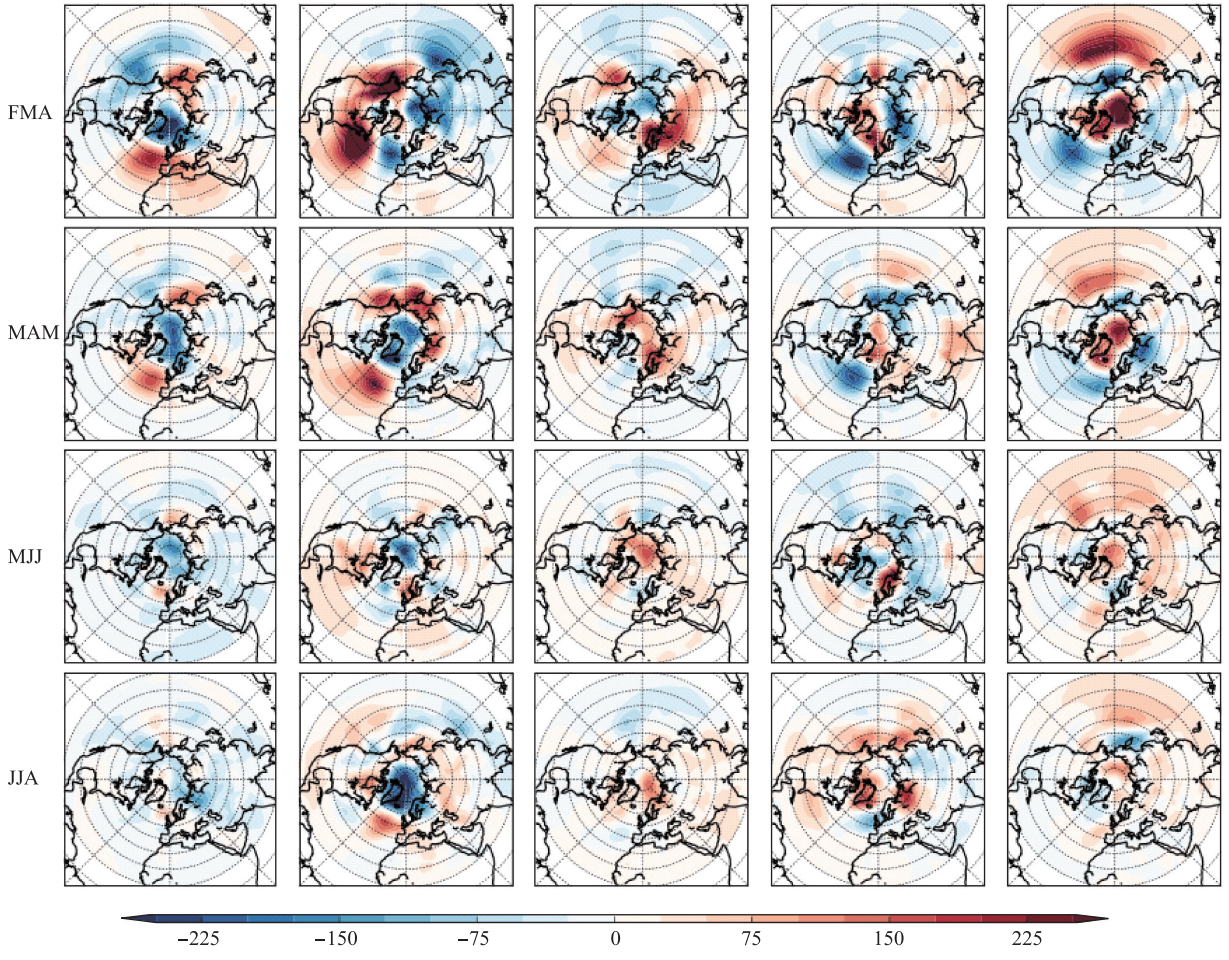

Figure 3 Monthly ERA-Interim mean sea level pressure anomaly (MSLPA) composites in Pa mapped to the SICA patterns of Figure 1. The first row represents composites occurring one month earlier than the corresponding SICA patterns, in the second row MSLPA composites occur in same months than SICA patterns, in the third row MSLPA composites occur two months later than SICA patterns and in the lowest row MSLPA composites occur three months later than SICA patterns.

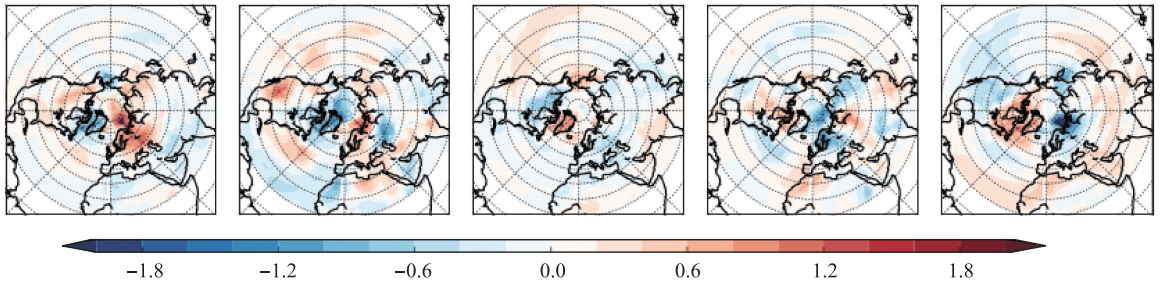

Figure 4 Detrended monthly ERA-Interim 2 metre surface air temperature anomalies (SATA) in MAM mapped to SOM patterns in Figure 1. Units are in K. Note the clear distinction between regions of cold anomalies associated with positive SICA patterns in Figure 1 and regions of warm anomalies associated with negative SICA patterns.

3.4 Atmospheric circulation and rainfall in China in JJA

MSLPA composites can be used to explain atmospheric large-scale circulation patterns related to extreme rainfall anomalies in China in JJA. For example, the rainfall composite (3,0) in Figure 2 is associated with a positive MSLPA in the Sea of Okhotsk and a negative MSLP over Northeast China (Figure 3, the lowest row and the fourth column from left). This horizontal MSLPA gradient enhances moist on-land air flow from the Pacific and results in the increase of extreme precipitation in Northeast China (Figure 2, the rainfall composite (3,0)). Contrary to this, the MSLPA composite associated with (3,0) favours dry air flow from the west to southeastern China due to the positive MSLPA over northeast Europe and due to the negative MSLPA over east Asia. Supporting this, the large-scale circulation composites related to the SICA pattern (3,0) (the third column in Figure 3) show a positive MSLPA, over north Europe persisting from MAM to JJA. This persistent positive MSLPA is related to positive SICA and negative near surface temperature anomalies (Figures 1, 4 and 5, third columns from left).

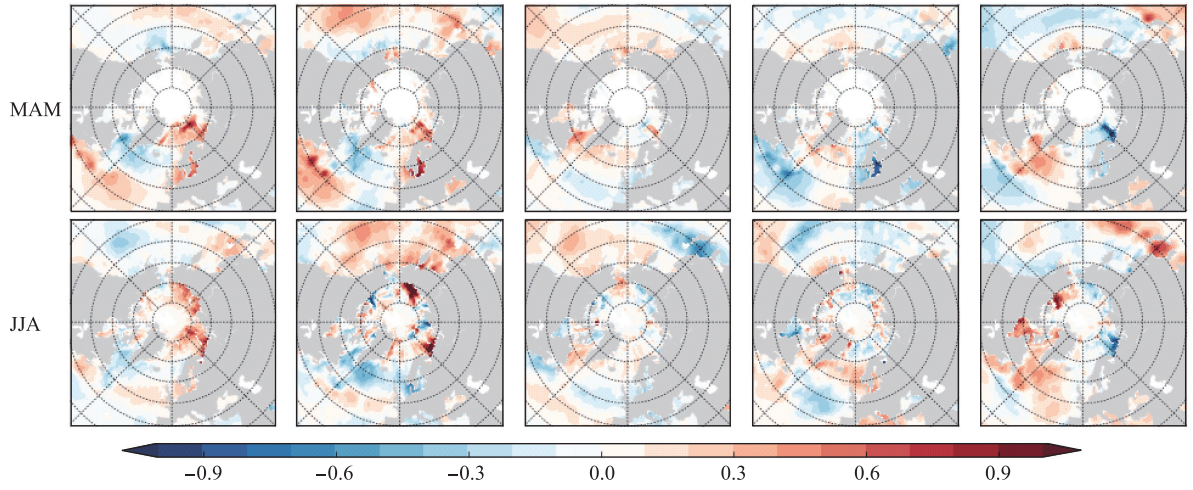

Figure 5 Detrended monthly HadISST sea-surface temperature anomaly (SSTA) composites mapped to the SICA patterns of Figure 1. The first row represents composites occurring in same months (MAM) than SICA patterns and the second row SSTA composites occurring three months later than SICA patterns.

The opposite is true for the rainfall composite (4,0) where the negative MSLPA occurs over the Sea of Okhotsk and the positive MSLPA occurs over Northeast China (Figure 3, the lowest row and the rightmost column). Now, the positive precipitation anomalies in composite (4,0) are related to the enhanced marine air flow to Southeast China, and might be further strengthened by high SSTA southeast of Japan (the lowest row and the rightmost column of Figure 5). Note that for the rainfall composite (4,0), no persistent positive MSLPA exists in north Europe (Figure 3, the rightmost column). In summary, large-scale circulation anomalies that favour dry off-land air flow in North China are related to a decrease in regional rainfall while simultaneously moist on-land air flow from the Pacific is likely to occur in South China. In South

China, atmospheric circulation anomalies are also associated with Pacific SSTA.

According to Zhao et al.[8], a reduced spring sea-ice extent in the Sea Okhotsk and the Bering Sea causes an anomalous high over Europe. This is visible in SICA patterns (2,0) and (3,0) which show negative or weakly positive SICAs in the Sea of Okhotsk and in the Bering Sea associated with MSLPA composites showing positive anomalies over Europe (Figure 3, third and fourth columns). In JJA, however, the MSLPA composite related to pattern (2,0) is positive over East Asia, compared to MSLPA composite related to (3,0) which results in a different rainfall response in China. Wu et al.[9] attributed rainfall anomalies in China to atmospheric wave train structures triggered by persistent spring-to-summer SICAs. As shown in Figure 5, such persistent SST anomalies exist in the Barents Sea, in the north Atlantic and in the Pacific related to SICA patterns (0,0), (1,0), (3,0) and (4,0). Guo et al.[10] revealed a mediating role of the North Pacific SSTs, which persistence is again demonstrated in Figure 5 as SSTA composites associated with SICA patterns (0,0) and (4,0) show unchanging and opposite SSTA composite patterns in the North Pacific from MAM to JJA. These SSTAs persisting from MAM to JJA modify the large-scale atmospheric circulation in JJA which then affects the rainfall in China.

3.5 Rainfall in JJA associated with the DJF sea-ice concentration anomaly SOM

Figure 6 shows SICA patterns in DJF and Figure 7 associated changes in rainfall extremes over Eurasia. Generally, during high sea ice conditions in the Labrador Sea (SICA pattern (0,0)) the rainfall in summer increases over a region extending from northeast Europe south-eastwards to mid-latitude East Asia, while the opposite is true for low Labrador sea ice conditions (see SICA pattern (3,0)). As was the case for SICA in MAM (Figure 1), South China experiences the opposite rainfall response than northern China (Figure 6, compare patterns (0,0) and (3,0)). These results are consistent with Wu et al.[11], who compared differences in summer rainfall between heavy and light sea-ice cases.

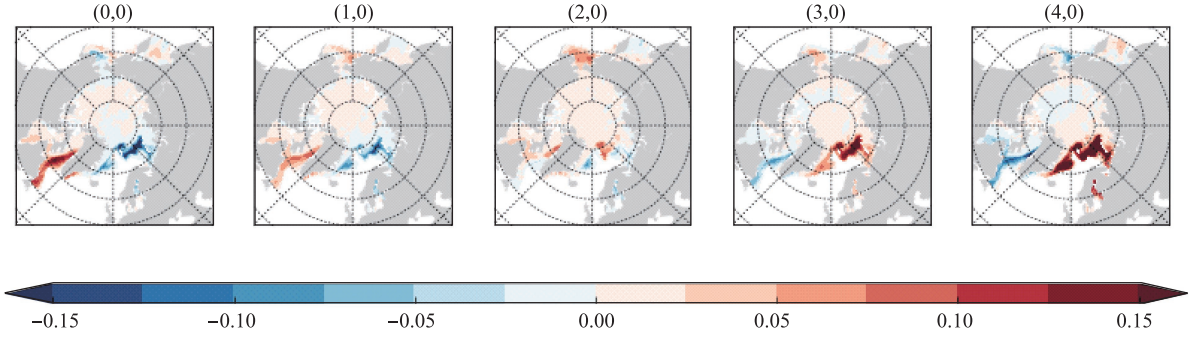

Figure 6 As Figure 1 but for DJF.

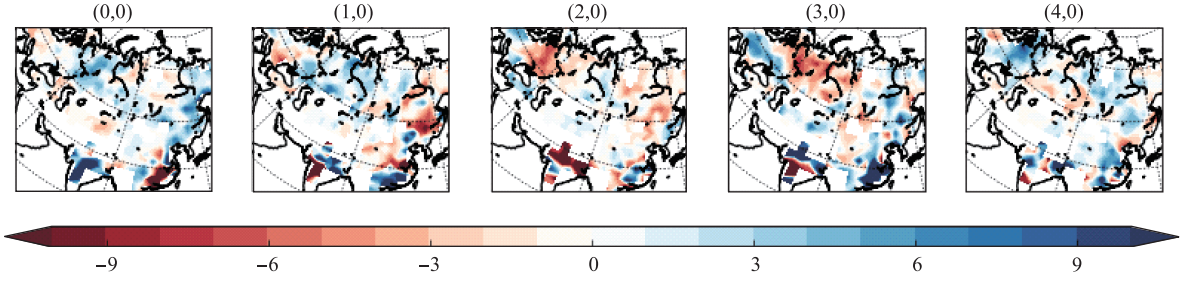

Figure 7 As Figure 2, but RX5day anomalies are mapped to the SOM of Figure 6.

The spring SICA may appear to be associated with summer rainfall in China in the opposite way than the winter SICA. Namely, high spring Arctic SICA, particularly in the Greenland Sea, is associated with reduced summer rainfall in North China while high winter SICA in the Labrador Sea is associated with increased summer rainfall in North China (compare Figures 1 and 2 pattern (4,0), and Figure 6 and 7 pattern (0,0)). The reason for this perhaps counterintuitive difference, as one expects these SICAs persist from winter to spring, lies in the opposite regional SICA patterns. In Figure 6, pattern (0,0) shows positive SICAs in the Labrador Sea in DJF when the Barents and Greenland seas SICAs are strongly negative. However, we should compare Figure 5 (0,0) pattern with Figure 1 (0,0) pattern where both MAM and DJF SICAs in the Labrador Sea are positive, or Figure 5 (4,0) pattern with Figure 1 (4,0) pattern where DJF and MAM SICAs in the

Labrador Sea are negative, because strong anomalies such as these persist until MAM (not shown). Therefore, we conclude that strong SICAs in the Labrador Sea and in the Greenland Sea typically persist from winter until spring. In this way, associations of rainfall composites with SICA patterns in DJF and in MAM become approximately similar.

3.6 Sea ice concentration, atmospheric circulation and surface temperatures in MAM

As shown on the first row of Figure 8, the driver for SICA in DJF, as in MAM, is the atmospheric circulation which indicates a high pressure in the eastern Arctic associated with cold air temperatures (not shown) and high SICAs in the Barents and Greenland Seas (the two rightmost patterns in Figure 6). Correspondingly, temperature anomalies, including SSTAs in Figure 9, are positive during negative SICAs (Figure 6) due to the warm advection from the Atlantic and from the Pacific (the two leftmost MSLPA composites in DJF in Figure 8). In the Labrador Sea, positive (negative) pressure anomaly east of North America is related to positive (negative) SICA enhancing the flow of cold continental air to the region, but in the Barents Sea, these MSLPA composites result in the opposite effect on SICAs. Generally, large-scale relationships between MSLPA and SICA in DJF resemble the ones in MAM.

In MAM, MSLPA composites associated with DJF SICA patterns (0,0) and (4,0) in Figure 8 (middle row) show many similar large-scale circulation characteristics than MSLPA composites associated with MAM SICA patterns (0,0) and (4,0) in Figure 3. This similarity also indicates resembling relationships between SICA in DJF and summer rainfall in China, and between SICA in MAM summer rainfall in China. Indeed, summer rainfall composites corresponding to MAM and DJF SICA patterns (0,0) show positive anomalies in Northeast China and negative anomalies in Southeast China, while rainfall composites corresponding to MAM and DJF SICA patterns (4,0) show negative anomalies in Northeast China and positive ones in Southeast China (compare Figures 2 and 7). The reason for these similarities lies in the winter-to-spring persistence of SICA patterns and associated SSTA composites (Figure 9).

The persistence of the strongest SICA patterns (0,0) and (4,0) and corresponding SSTA composites from winter to spring and further to summer is crucial for the establishment of linkages between these SICAs and summer rainfall in China. SSTA composites are illustrated in Figure 9, where the leftmost column displays a sequence of SSTA composites related to DJF SICA pattern (0,0) showing negative SSTAs in the Labrador Sea and positive SSTAs in the Barents and Greenland seas persisting from DJF to JJA. Equivalently, the sequence of SSTA composites in the rightmost column related to DJF SICA pattern (4,0) displays approximately the opposite SSTA anomalies than the leftmost column. In the North Pacific, the persistence of SSTAs appears shorter than in the Labrador Sea, in the Barents Sea and in the Greenland Sea. East of Japan, strong positive SSTAs are preceding the

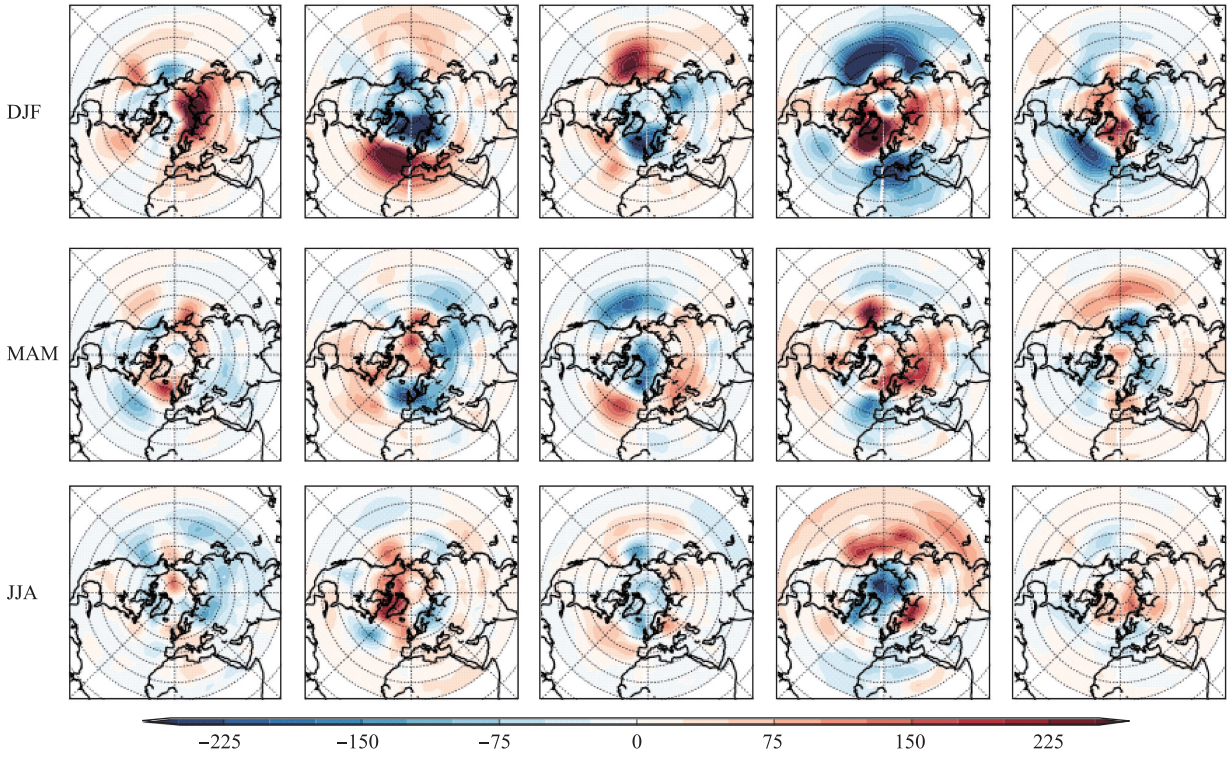

Figure 8 As Figure 3, but for SOM of Figure 6 and with rows extending from DJF to JJA.

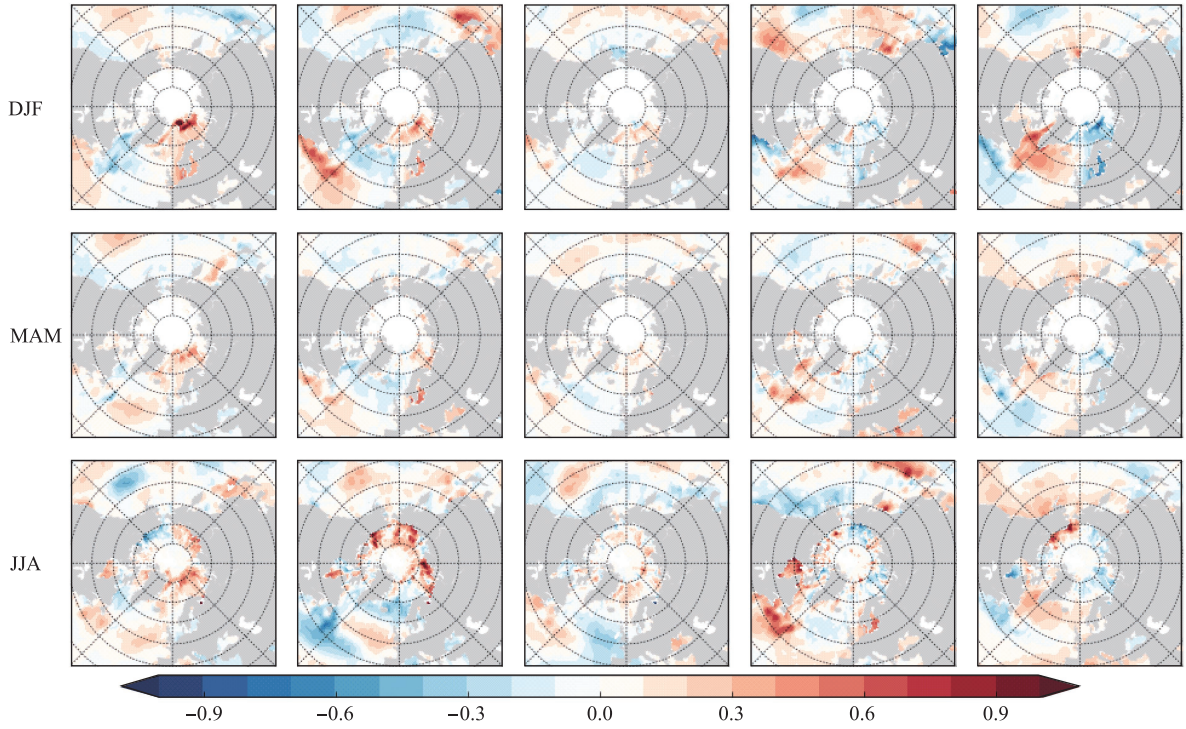

Figure 9 As Figure 5, but SSTAs are mapped to SOM of Figure 6 and with rows extending from DJF to JJA.

increased extreme rainfall in Southeast China as can be seen by comparing the rainfall composite associated with pattern (3,0) in Figure 7 and the corresponding SSTA composite of Figure 9 in JJA. Regarding previous studies, our findings related to the North Atlantic SSTA persistence are consistent with Wu et al.[11] who emphasised the mediator role of the horseshoe-like SST pattern curving around south Greenland. In our analysis, this pattern is visible from DJF to JJA in composites associated with SICA patterns (0,0) and (4,0) in both Figures 5 and 9.

4 Conclusions

We associated extreme rainfall events, mean sea level pressure, near surface air temperature and sea surface temperature composites with five Arctic sea-ice concentration patterns classified by using the Self-Organising Maps technique. Several new relationships could be identified, for instance in India and Europe, but their closer examination is out of the scope of this study and is considered as future work. The significance of these new relationships could be tested by using already identified relationships in this study as the reference metric.

We plotted sequences of mean sea level pressure and sea surface temperature composites representing the evolution of large-scale atmospheric circulation patterns and the persistence of sea surface temperature features from winter to summer to gain further understanding on the preconditioning leading to extreme rainfall anomalies in China. The evolution of atmospheric circulation and the persistence of sea surface temperature and sea-ice concentration patterns led to resembling extreme rainfall responses in China in case of strongest initial sea-ice concentration anomalies both in winter and in spring. For example, we identified that high (low) winter and spring sea-ice conditions in the Labrador Sea result in increased (decreased) extreme precipitation in Northeast China. The reason for this similar behaviour lies in sea-ice concentration and sea surface temperature anomalies that persist from winter to spring and further to summer. These persisting anomalies then alter the large-scale atmospheric circulation which impacts the rainfall in China. Also this topic deserves a closer examination in the future.

After a careful interpretation of our SOM based results, we are able to largely confirm individual links between the Arctic sea ice and the rainfall in China as found in earlier studies and as summarised in Table 1. On the other hand, our SOM analysis indicates that previous studies might be biased towards anomalies in specific regions, while our analysis suggests more complex relationships associated with specific Arctic-wide sea-ice concentration anomaly patterns. To confirm these relations, model simulations and subsequent analysis would be required.

Acknowledgments The ECMWF is acknowledged for providing us with the ERA-Interim results and Hadley Centre, the UK, for providing us with the HadISST data. We thank the WMO CCl/CLIVAR/JCOMM Expert Team on Climate Change Detection and Indices (ETCCDI), the CLIMDEX project and the Australian Research Council Linkage Grant LP100200690 for providing us the HadEX2 data. The work was supported by the Academy of Finland (contract 259537). We thank two anonymous reviewers for their very valuable comments on the manuscript.

References

1 Parkinson C L, Comiso J C. On the 2012 record low Arctic sea ice cover: Combined impact of preconditioning and an August storm. Geophysical Research Letters, 2013, 40: 1356–1361, doi:10.1002/grl.50349.

2 Smedsrud L H, Esau I, Ingvaldsen R B, et al. The role of the Barents Sea in the Arctic climate system. Reviews of Geophysics, 2013, 51: 415-449, doi:10.1002/rog.20017.

3 Miles M, Divine D. A signal of persistent Atlantic multidecadal variability in Arctic sea ice. Geophysical Research Letters, 2014, 41: 463–469, doi:10.1002/2013GL058084.

4 Vihma T. Effects of Arctic sea ice decline on weather and climate: a review. Surveys in Geophysics, 2014, 35: 1175–1214, doi:10.1007/s10712-014-9284-0.

5 Francis J A, Vavrus S J. Evidence linking Arctic amplification to extreme weather in mid-latitudes. Geophysical Research Letters, 2012, 39 (L06801), doi:10.1029/2012GL051000.

6 Uotila P, Vihma T, Tsukernik M. Close interactions between the Antarctic cyclone budget and large–scale atmospheric circulation. Geophysical Research Letters, 2013, 40: 3237-3241, doi:10.1029/50560.

7 Barnes E A, Dunn-Sigouin E, Masato G, Woollings T. Exploring recent trends in Northern Hemisphere blocking. Geophysical Research Letters, 2014, 41: 638–644, doi:10.1002/2013GL058745.

8 Zhao P, Zhang X D, Zhou X J, et al. The sea ice extent anomaly in the North Pacific and its impact on the East Asian summer monsoon rainfall. Journal of Climate, 2004, 17: 3434–3447.

9 Wu B Y, Zhang R H, Wang B, et al. On the association between spring Arctic sea ice concentration and Chinese summer rainfall. Geophysical Research Letters, 2009: 36 (L09501), doi:10.1029/2009GL037299.

10 Guo D, Gao Y Q, Bethke I, et al. Mechanism on how the spring Arctic sea ice impacts the East Asian summer monsoon. Theoretical and Applied Climatology, 2013, 115: 107–119, doi:10.1007/s00704-013-0872-6.

11 Wu B Y, Zhang R H, D'Arrigo R et al. On the Relationship between winter sea ice and summer atmospheric circulation over Eurasia. Journal of Climate, 2013, 26: 5523–5536, doi:10.1175/JCLI-D-12-00524.1.

12 Chen M, Xie P, Janowiak J E, et al. Global land precipitation: A 50-yr monthly analysis based on gauge observations. Journal of Hydrometeorology, 2002, 3: 249–266.

13 Kohonen T. Self-Organizing Maps. New York: Springer, 2001.

14 Hewitson B C, Crane R G. Self-Organising Maps: Applications to synoptic climatology. Climate Research, 2002, 22: 13–26.

15 Cassano J J, Uotila P, Lynch A H. Changes in synoptic weather patterns in the polar regions in the 20th and 21st centuries. Part 1: Arctic. International Journal of Climatology, 2006, 26: 1027–1049, doi:10.1002/joc.1306.

16 Lynch A H, Uotila P, Cassano J J. Changes in synoptic weather patterns in the polar regions in the 20th and 21st centuries, Part 2: Antarctic. International Journal of Climatology, 2006, 26: 1133–1281, doi:10.1002/joc.1305.

17 Uotila P, Lynch A H, Cassano J J, et al. Changes in Antarctic net precipitation in the 21st century based on Intergovernmental Panel on Climate Change (IPCC) model scenarios. Journal of Geophysical Research, 2007, 112 (D10107), doi:10.1029/2006JD007482.

18 Skific N, Francis J. Self-Organizing Maps: A powerful tool for the atmospheric sciences, applications of Self-Organizing Maps. Magnus Johnsson (Ed.), InTech, 2012: 251-268, doi:10.5772/54299.

19 Alexander L V, Uotila P, Nicholls N. Influence of sea surface temperature variability on global temperature and precipitation extremes. Journal of Geophysical Research, 2009, 114 (D18116), doi:10.1029/2009JD012301.

20 Rayner N A, Parker D E, Horton E B, et al. Global analyses of sea surface temperature, sea ice, and night marine air temperature since the late nineteenth century. Journal of Geophysical Research, 2003, 108: 4407, doi:10.1029/2002JD002670.

21 Huva R, Dargaville R, Rayner P. The impact of filtering Self-Organising Maps: a case study with Australian pressure and rainfall. International Journal of Climatology, 2014, doi:10.1002/joc.4008.

22 Donat M G, Alexander L V, Yang H, et al. Updated analyses of temperature and precipitation extreme indices since the beginning of the twentieth century: The HadEX2 dataset. Journal of Geophysical Research, 2013, 118: 2098–2118. doi:10.1002/jgrd.50150.

23 Dee D P, Uppala S M, Simmons A J, et al. The ERA-Interim reanalysis: Configuration and performance of the data assimilation system. Quarterly Journal of the Royal Meteorological Society, 2011, 137: 553–597, doi:10.1002/qj.828.

24 Hodges K I, Lee R W, Bengtsson L. A comparison of extra-tropical cyclones in recent re-analyses; ERA-INTERIM, NASA-MERRA, NCEP-CFSR and JRA25. Journal of Climate, 2011, 24: 4888–4906, doi:10.1175/ 2011JCLI4097.1.

25 Simmons A J, Poli P. Arctic warming in ERA-Interim and other analyses. Quarterly Journal of the Royal Meteorological Society, 2014, doi:10.1002/qj.2422.

26 Cornes R C, Jones P D. How well does the ERA-Interim reanalysis replicate trends in extremes of surface temperature across Europe? Journal of Geophysical Research, 2013 118: 10,262–10,276, doi:10.1002/jgrd.50799.

27 Walker G T. Correlation in seasonal variations of weather, VIII: A preliminary study of world weather. Mem Ind Meteor Dept (Poona), 1923, 24: 275–332.

28 Thompson D, Wallace J M. The Arctic Oscillation signature in the wintertime geopotential height and temperature fields. Geophysical Research Letters, 1998, 25: 1297-1300.